Editors' Suggestion | Featured in Physics

# Self-Ordering of Buckling, Bending, and Bumping Beams

Arman Guerra,[1] Anja C. Slim,[2,3] Douglas P. Holmes,[1] and Ousmane Kodio[4,5,*]
[1]Department of Mechanical Engineering, Boston University, Boston, Massachusetts 02215, USA
[2]School of Mathematics, Monash University, Clayton Victoria 3800, Australia
[3]School of Earth, Atmosphere and Environment, Monash University, Clayton Victoria 3800, Australia
[4]Department of Mathematics, Massachusetts Institute of Technology, Cambridge, Massachusetts 02139, USA
[5]Department of Mechanical Engineering, University of California, Santa Barbara, California 93106, USA

(Received 19 October 2022; accepted 7 February 2023; published 3 April 2023)

A collection of thin structures buckle, bend, and bump into each other when confined. This contact can lead to the formation of patterns: hair will self-organize in curls; DNA strands will layer into cell nuclei; paper, when crumpled, will fold in on itself, forming a maze of interleaved sheets. This pattern formation changes how densely the structures can pack, as well as the mechanical properties of the system. How and when these patterns form, as well as the force required to pack these structures is not currently understood. Here we study the emergence of order in a canonical example of packing in slender structures, i.e., a system of parallel confined elastic beams. Using tabletop experiments, simulations, and standard theory from statistical mechanics, we predict the amount of confinement (growth or compression) of the beams that will guarantee a global system order, which depends only on the initial geometry of the system. Furthermore, we find that the compressive stiffness and stored bending energy of this metamaterial are directly proportional to the number of beams that are geometrically frustrated at any given point. We expect these results to elucidate the mechanisms leading to pattern formation in these kinds of systems and to provide a new mechanical metamaterial, with a tunable resistance to compressive force.

DOI: 10.1103/PhysRevLett.130.148201

When thin structures pack, there is a competition between elasticity, which often encourages pattern formation and densification, and geometric constraints. For example, paper, when crumpled into a ball, forms complex three-dimensional swirls [1,2], and DNA strands inserted into cell nuclei fold and pack into layers [3,4]. In some cases, these densification processes are resisted by friction [5,6] and geometrical incompatibilities in the deformation of the materials [7–10]. The formation of patterns has been studied thoroughly in cases where thin structures are adhered to a substrate [11–14], sheets are constrained in a ring [6,15,16], and rods are inserted into a container [17–19]. However, the question of to what degree the rods and sheets will order themselves in these complex and random packing processes is still open.

In structured arrangements of elastic beams, the competition between order and geometric frustration has been used to great effect in the design of materials with novel and programmed properties [20–23]. There are many models in statistical mechanics to rationalize the emergence of order [24,25], and in some cases these models have been extended to study frustration, fluctuation, and shape change in thin elastic structures [26–29]. However, these models are insufficient to capture the ordering of beams because of the difficulty of finding and modeling the interaction forces between adjacent elements. For example, consider a simple 1D version of the ordering of packed beams, the gills of a mushroom [see Fig. 1(a)]. If the mushroom dries and shrinks, the gills will at first buckle and then bump into each other. Reminiscent of the 1D Ising model for magnetism [24], the ground state of this system occurs when all gills point in the same direction [shown in an

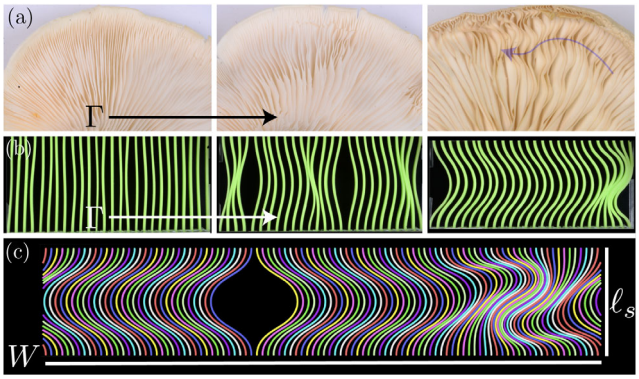


FIG. 1. (a) An oyster mushroom that has been left in the open air to dry (approximately one day between consecutive pictures). During this drying process, the gills become compressed along their length, causing them to buckle (middle) and then align (right). (b) Experimental observations of a similar phenomenon in a system of slender parallel plates compressed in an Instron. (c) A numerical experiment of the same system. Videos of a typical experiment (Supplemental Material, Video 1 [30]) and simulation (Supplemental Material, Video 2) are available.

 

analogous experiment in Fig. 1(b), right]. However, here there exists a hierarchy of disordered metastable states in the shallow-postbuckling regime, where the gills self-organize into "clumps" and leave "holes" where they have separated [Fig. 1(a), middle].

In this Letter, we consider a simplified version of this system: an array of $N$ parallel elastic beams confined to a vertical space $\ell_s$ that is shorter than their length $\ell$ and equally spaced inside of a box of width $W$, such that the distance between the centers of any two adjacent beams is $d = W/N$ [Fig. 1(c)]. We characterize the control parameter of the system to be the confinement factor $\Gamma = \ell/\ell_s$. If the beams are initially perturbed in random directions, we observe behavior reminiscent of a phase transition, where the initial disordered state (beams buckled in random directions) will gradually decay to the fully ordered ground state (all beams aligned in one direction) as $\Gamma$ increases. We therefore ask the following two questions: First, when and how much will the beams align; can we predict how order will emerge? Second, how does the mechanical response of the system depend on the degree of order and its emergent topology; conversely, could we use this emergent topology in the design of tunable-stiffness materials?

To investigate this state transition experimentally, we built a stiff acrylic two-piece mount that served to clamp many slender elastic plates at two of their opposite edges (effecting clamped-clamped boundary conditions). We inserted sheets of polyvinyl siloxane (thickness $h = 1.5$ mm, number $N = 26$) into the mounts and compressed the system uniformly with an Instron, which allowed us to measure $\Gamma$, as well as the force response of the arrangement of beams [Fig. 1(b)]. We then performed an ensemble of nonthermal quenches on this array of beams; that is, we isostatically compressed the beams many times, manually biasing each beam by hand to initially buckle to the right or left based on a random coin flip at the start of each experiment (further details in the Supplemental Material, Sec. I [30]). Just as we see in the case of the mushroom [Fig. 1(a)], any adjacent beams buckling toward each other will eventually make contact and form clumps [Fig. 1(b), middle]. After enough confinement, these clumps become unstable and decompose, and the beams eventually all point in one direction [Fig. 1(b), right].

We parametrize the direction of the buckling of each beam using what we call the "tropism," where $T_i = 0$ when beam $i$ is unbuckled, and $T_i = +1$ $(-1)$ if it is buckled to the right (left), as shown in Fig. 2(a). To account for beams that are no longer in the first buckling mode because of contact with other adjacent beams or with the walls, we consider that a beam is buckled to the right (left) if the portion of the beam halfway up the box is farther to the right (left) than its ends. We can average the behavior of all beams into an overall system tropism,

$$\bar{T} = \left| \frac{1}{N} \sum_{i=1}^{N} T_i \right|. \tag{1}$$

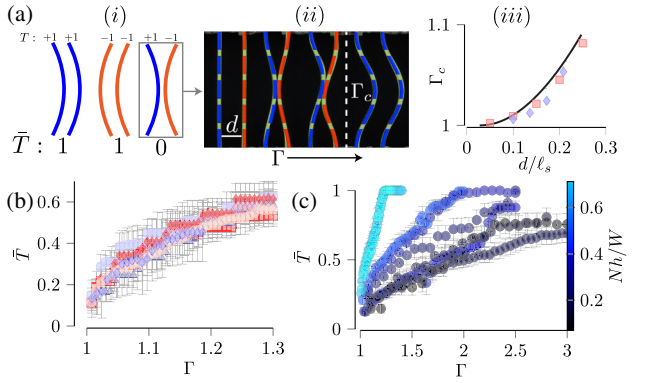


FIG. 2. The emergence of order for (a) two beams and (b),(c) many beams. (a),(i) Illustrated examples of $T_i$ (+1, blue; −1, orange) (a),(ii) Experiments (green) overlaid with simulations (blue and orange) of two beams that buckle toward each other. There are two metastable "clumped" $\bar{T} = 0$ states (vertically and rotationally symmetric), however, when $\Gamma > \Gamma_c$, $\bar{T} = 1$. (a), (iii) $\Gamma_c$ increases with the normalized distance between two beams $d/\ell_s$ (experiments, blue diamond; simulations, red square; model, black line; Supplemental Material, Sec. II [30]) (b) $\bar{T}$ for experiments and simulations of many beams ($N = 26$, $W = 140$ mm, $\ell_s = 54$ mm, $h = 1.54$ mm, average $d = 5.4$ mm, number of ensemble measurements: experiment, 25; simulation, 100) (c) $\bar{T}$ increases with $\Gamma$ with a rate highly dependent on $N$, $d$, $W$, $h$, and $\ell_s$.

Note that $\bar{T} \approx 0$ when the beams are randomly directed, and $\bar{T} \approx 1$ when the beams are all aligned [Fig. 1(b), right]. We plot the ensemble average of $\bar{T}$ at increasing $\Gamma$ for a fixed beam spacing, number, thickness, and initial length in Fig. 2(b) (blue diamond) and indeed find a gradual increase in the average order of the system. We find that order arises at different $\Gamma$ for different random initializations of the beam buckling directions, so we use error bars to indicate the 95% confidence interval for the ensemble-average $\bar{T}$ (found using a bootstrap method [31]) We can compare this with the behavior of two beams buckling toward each other [Figs. 2(a)(ii) and 2(a)(iii)] and find that for the many-beam case, the clumps remain stable (and therefore $\bar{T} < 1$) at much higher $\Gamma$ for the same normalized beam spacing $d/\ell_s$ [Fig. 1(c)].

To eliminate any imperfections in the experimental setup and other forces such as gravity, we replicated the geometry of our physical experiments using numerical experiments [ensemble $\bar{T}$ shown in Fig. 2(b), blue triangle] in the Large-Scale Atomic/Molecular Massively Parallel Simulator ([32], visualizations in OVITO [33]) adopting a similar protocol as [34] to simulate the mechanics of the elastic beams (Supplemental Material, Sec. III [30]). We also include simulations with varying coefficient of sliding friction ($\mu_s = 0$, frictionless, red square; $\mu_s = 1$, rubberlike, purple diamond; $\mu_s = 2$, highly frictional, dark red diamond) and different beam end (pin-pin, blue circle) and vertical box edge (periodic, red square) boundary conditions. Additionally, we performed simulations where

the distances between the beams were uniformly randomly distributed with a lower bound of $1.2h$ and an upper bound such that the average distance between the beams is the same as the model experiment (Supplemental Material, Video 3, pink circle [30]). We find good agreement between experiments and simulations, and furthermore the tropism $\bar{T}$ is statistically independent of the degree of friction, boundary conditions, and beam spacing variability. The lack of dependence on friction is somewhat unique when compared to other work on the packing of slender structures [5,6,15–19]. However, our setup is designed specifically to study the emergence of order, not the packing of the elastic structures in space. In our system, order arises at relatively low confinement compared to other studies, and since understanding this ordering is our aim, we do not consider a highly packed regime, where the beams would begin to slide against each other and the walls, and friction would play a larger role. We discuss this further in Sec. IV of the Supplemental Material [30]. Hence, without loss of generality, we performed simulations of clamped-clamped, evenly spaced beams without friction in a periodic box, with the expectation that the results apply broadly. We varied the beam density as well as the number of beams, plot $\bar{T}$ as a function of $\Gamma$ in Fig. 2(c), and find that $\bar{T}$ strongly depends on the geometric parameters of the box.

In Fig. 3(a), we show a series of simulations with increasing $\Gamma$. We find that beams align when clumps and holes "meet" and annihilate; that is, the space between the center of a clump and a hole is completely taken up by the horizontal deflection of the hole ($d_h$) and the clump ($d_c$), as well as the sum of the thicknesses of the beams between them [Fig. 3(b), more detail in the Supplemental Material, Sec. V [30] ]. We can use this mechanism to predict $\bar{T}$ as a function of $\Gamma$. We would expect that $\bar{T} = 1$ when the final clump meets and annihilates with the final hole. For simplicity, we will consider the case where the edges of the box are periodic, and as such, the maximum

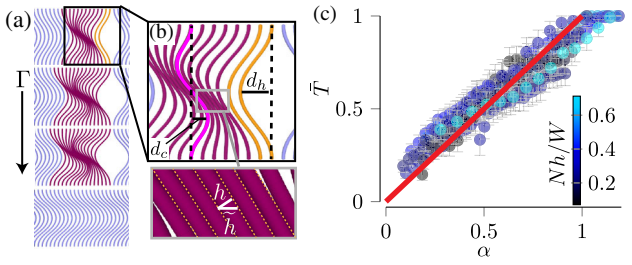


FIG. 3. Understanding beam alignment. (a) A step-by-step illustration of clump-hole annihilation, with simulations at increasing $\Gamma$ from top to bottom. Clumped beams are colored purple, and all others are colored by their tropism ($T_i = 1 \rightarrow$ blue, $T_i = -1 \rightarrow$ orange). (b) Illustration of the parameters in our mathematical model. (c) The ensemble value of $\bar{T}$ as a function of $\alpha$ [prediction from Eq. (2), red]. Error bars are the same as in Fig. 2(c), left off for clarity.

possible distance between the final clump-hole pair is $W/2$. If we approximate the shape of a beam as a triangle, using the Pythagorean theorem, $d_h \approx \frac{1}{2}\ell_s\sqrt{\Gamma^2 - 1}$. We can further approximate the center beam of a clump as a mode-2 buckled elastica, and so $d_c \approx d_h/2$.

In experiments and simulations, we observe that clumps and holes do not move laterally as the beams are confined, and therefore, before annihilation, the number of beams between a clump and a hole $N_b$ stays the same. However, the effective horizontal thickness $\tilde{h}$ of the beams changes, as shown in Fig. 3(b). If we keep our triangular approximation for the shape of the beams, we get that $\tilde{h} \approx h\Gamma$ and therefore the additional space that each beam takes up is $\tilde{h} - h = h(\Gamma - 1)$.

When the maximum amount of initially empty space between a clump and a hole $(W/2 - Nh/2)$ is taken up by these three previously mentioned lengths $[d_h + d_c + N_b h(\Gamma - 1)]$, all clumps and holes will have met and annihilated, and $\bar{T} \rightarrow 1$. In the case where the last clump and hole are as far apart as they can be, $N_b = N/2$, so the fraction of the horizontal space between the clump and hole taken up by the beams, which we will call the "porosity" $\alpha$, is $\alpha = [d_h + d_c + N(\tilde{h} - h)/2]/(W/2 - Nh/2)$. In Fig. 3(c), we plot $\bar{T}$ against $\alpha$ and find that, as we expect, for all geometries, $\bar{T} \approx 1$ when $\alpha = 1$. More than that, however, it seems that the tropism is *approximately equal* to $\alpha$, or in other words, rearranging and inserting our previously derived values for the clump and hole deflections,

$$\bar{T} \approx \alpha = \frac{\frac{1}{2}(\Gamma - 1)hN + \frac{3}{4}\ell_s\sqrt{\Gamma^2 - 1}}{W/2 - Nh/2}. \tag{2}$$

This comes from the fact that, as the beams are confined, the number of clumps and holes that make contact and annihilate is proportional to the space that the beams take up. We note that, as can be seen from Fig. 3(c), even when $\alpha = 1$, there are some cases where $\bar{T}$ is slightly less than 1. We expect that these small discrepancies come from the fact that, rather than explicitly deriving $d_h$, $d_c$, and $\tilde{h}$, we have approximated their values. A more thorough theoretical treatment of the beams might improve the quality of our prediction; however, we believe that these approximations are sufficiently elucidating for the purposes of this Letter.

Now that we understand when the beams will become ordered, we turn to our second question: how do the beams respond to the imposed compression when they are not ordered? This is analogous to why it requires less force to confine paper to a target volume through folding than through crumpling [2]: A larger degree of geometrical frustration in thin structures often leads to more stored energy [35]. We can observe this directly in our system. In Fig. 4, we plot the normalized compressive force $\tilde{F}_i = F_i/F_1$ of each beam in a clamped-clamped, periodic,

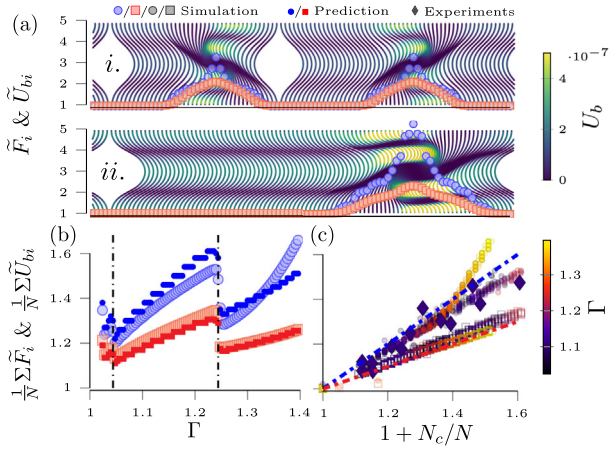


FIG. 4. Ordering affects compressive stiffness. (a) Snapshots of a simulation at $\Gamma = 1.18$ (i) and $\Gamma = 1.38$ (ii), superimposed with the vertical compressive force ($F_i$, blue circle) and bending energy ($U_{bi}$, red square) of each beam, normalized by the force and bending energy of a beam that is not part of a clump ($F_1$, $U_{b1}$). (b) The total compressive force (blue circle) and bending energy (red square) of the same system of beams as a function of $\Gamma$, normalized by the compressive force and bending energy of the system if all the beams were buckled in the same direction. Predictions from our approximated model [Eq. (3)] are blue filled circle ($F$) and red filled square ($U_b$). Vertical lines show places where a clump and hole annihilate (Supplemental Material, Video 4 [30]). (c) Normalized force and bending energy against $1 + N_t/N$ together with our predictions from Eq. (3) (simulation $U_b$, squares; predicted $U_b$, red line; simulation $F$, circles; experiment $F$, diamonds; predicted $F$, blue line). Gray in the legend indicates coloration by $\Gamma$.

frictionless simulation, where $F_i$ is the compressive force applied to beam $i$, and $F_1$ is the compressive force applied to a single beam with the same boundary conditions, compressed to the same $\Gamma$ and no neighboring beams. We simultaneously define and plot the normalized bending energy $\tilde{U}_{bi} = U_{bi}/U_{b1}$ in the same way, where $U_{bi}$ is the bending energy of beam $i$, and $U_{b1}$ is the corresponding bending energy of the beam from which we derive $F_1$. We superimpose these plots onto the simulated configurations. For beams that are not in clumps, and therefore have no contacts, $\tilde{F}_i = \tilde{U}_{bi} = 1$. In contrast, beams that are in contact with other beams in a clump and are geometrically frustrated [35] have a higher $\tilde{F}_i$ and $\tilde{U}_{bi}$, as they cannot find their lowest-energy state. These results indicate that our system is behaving like a mechanical metamaterial, an object that gets its properties not only from the material that it is made of, but also its internal geometry [23].

Previously, we noted that the beam at the center of a clump has the approximate shape of a mode-2 elastica. We would expect that $U_b \propto n$, where $n$ is the mode number of the beam (since doubling $n$ doubles the average curvature in the beam), so for the central beam in the clump, we expect that $\tilde{U}_{bi} \approx 2$. This is confirmed in Fig. 4(a), even for very large $\Gamma$. To estimate $F_i$ for the central beam of a clump, we performed additional simulations of a single beam, where the slope at the vertical center of the beam was forced to match the slope derived from our triangular approximation of the beam shape. In these simulations, we found that $\tilde{F}_i \approx 3$. In Fig. 4(a), we find that the maximum value of $\tilde{F}_i$ is indeed approximately 3 for most of the simulation, but increases for very large $\Gamma$, which we expect comes from a deviation of the true beam shape from our approximation.

In Fig. 4(a), we see that $\tilde{F}_i$ and $\tilde{U}_{bi}$ for the beams in the clump seem to increase linearly from $\approx 1$ at the edge of the clump to the maximum value at the clump center. If we use our earlier approximations for these maximum values ($\tilde{U}_{bi} \approx 2$ and $\tilde{F}_i \approx 3$), we might expect that, on average, a beam in a clump has $\tilde{U}_{bi} \approx 1.5$ and $\tilde{F}_i \approx 2$. Hence, we would expect that the total force and bending energy in our arrangement of beams is

$$F = F_1(N + N_c),$$
$$U_b = U_{b1}(N + N_c/2), \tag{3}$$

where $N_c$ is the number of beams that are in a clump. In Fig. 4(b), we plot the total normalized force $F/(NF_1)$ (blue circle) and bending energy $U_b/(NU_{b1})$ (red square) of the specific simulation run pictured in Fig. 4(a), along with their estimated values from the number of clumped beams as given by Eq. (3) and find good agreement, except at high $\Gamma$, when the normalized force estimate starts to fail, as we expected. In Fig. 4(c), we plot $F/(NF_1)$ (circles) and $U_b/(NU_{b1})$ (squares) against $1 + N_c/N$ and find that, for a wide variety of box geometries, $U_b/(NU_{b1})$ collapses to $(1 + N_c/N)/2$ for all data, and $F/(NF_1)$ collapses approximately to $1 + N_c/N$ for all data except for that at very high $\Gamma$, both of which reinforce the appropriateness of Eq. (3). We expect that this error in the prediction of $F/(NF_1)$ could be reduced with an analytical treatment of $\tilde{F}_i$ for the beam at the center of a clump (which may itself depend on $\Gamma$), which could replace the value of 3 that we approximated from the model simulation mentioned above.

In this Letter, we have studied how many parallel beams clamped at their ends and confined in a box order themselves and found that, at high enough $\Gamma$, $\bar{T} \to 1$. We also found that the compressive stiffness of the metamaterial made up of these buckling beams is proportional to the number of beams in a clump, potentially allowing the stiffness to be manually or automatically tuned. We expect that changes in the geometry that we have studied could lead to a large dependence on friction, as is the case in many other systems of slender contacting structures [5,36–40], creating an additional route for novel functionalities. Furthermore, any intrinsic thermal motion [29], adhesion [41,42], curvature, or any transverse loading or long-range potentials may affect the ordering and mechanical properties of the system, potentially providing deeper analogies to other work in statistical mechanics [25,26] and more tunability. So far, we have only considered beams with two motion-restricted

ends and fixed or periodic box edges; further studies could consider cases where one end of the beams is free (like hair, microtubules [43], or a carbon nanotube forest [44,45]) or restricted only by friction with a wall, or where a lateral edge is clamped, such as in the case of the mushroom gills. We also note that, as the beams are compressed, a transverse force (the compression) turns into a longitudinal transfer, namely, the redirection of the beams. This could provide a method to redirect and control mechanical waves [46,47].

We thank Abigail Plummer, Harold Park, and Dominic Vella for helpful discussion. We also gratefully acknowledge the financial support from DARPA (No. HR00111810004) and from NSF CMMI–CAREER through Mechanics of Materials and Structures (No. 1454153), and the computing resources of the Boston University Shared Computing Cluster.

*kodio@mit.edu

[1] A. D. Cambou and N. Menon, Proc. Natl. Acad. Sci. U.S.A. **108**, 14741 (2011).
[2] S. Deboeuf, E. Katzav, A. Boudaoud, D. Bonn, and M. Adda-Bedia, Phys. Rev. Lett. **110**, 104301 (2013).
[3] D. E. Smith, S. J. Tans, S. B. Smith, S. Grimes, D. L. Anderson, and C. Bustamante, Nature (London) **413**, 748 (2001).
[4] J. Kindt, S. Tzlil, A. Ben-Shaul, and W. M. Gelbart, Proc. Natl. Acad. Sci. U.S.A. **98**, 13671 (2001).
[5] H. Alarcón, T. Salez, C. Poulard, J.-F. Bloch, É. Raphaël, K. Dalnoki-Veress, and F. Restagno, Phys. Rev. Lett. **116**, 015502 (2016).
[6] S. Alben, Proc. R. Soc. A **478**, 20210742 (2022).
[7] J. Andrejevic, L. M. Lee, S. M. Rubinstein, and C. H. Rycroft, Nat. Commun. **12**, 1 (2021).
[8] G. Domokos, P. Holmes, and B. Royce, in *Mechanics: From Theory to Computation* (Springer, New York, 2000), pp. 413–446.
[9] B. Roman and A. Pocheau, Europhys. Lett. **46**, 602 (1999).
[10] A. Pocheau and B. Roman, Physica (Amsterdam) **192D**, 161 (2004).
[11] M. A. Biot, *Bending of an Infinite Beam on an Elastic Foundation* (American Society of Mechanical Engineers, New York, 1937).
[12] D. A. Dillard, B. Mukherjee, P. Karnal, R. C. Batra, and J. Frechette, Soft Matter **14**, 3669 (2018).
[13] O. Kodio, I. M. Griffiths, and D. Vella, Phys. Rev. Fluids **2**, 014202 (2017).
[14] O. Oshri, Y. Liu, J. Aizenberg, and A. C. Balazs, Phys. Rev. E **97**, 062803 (2018).
[15] L. Boué, M. Adda-Bedia, A. Boudaoud, D. Cassani, Y. Couder, A. Eddi, and M. Trejo, Phys. Rev. Lett. **97**, 166104 (2006).
[16] M. Adda-Bedia, A. Boudaoud, L. Boué, and S. Deboeuf, J. Stat. Mech. (**2010**) P11027.
[17] C. C. Donato and M. A. F. Gomes, Phys. Rev. E **75**, 066113 (2007).
[18] N. Stoop, J. Najafi, F. K. Wittel, M. Habibi, and H. J. Herrmann, Phys. Rev. Lett. **106**, 214102 (2011).
[19] R. Vetter, F. K. Wittel, and H. J. Herrmann, Nat. Commun. **5**, 4437 (2014).
[20] B. Florijn, C. Coulais, and M. van Hecke, Phys. Rev. Lett. **113**, 175503 (2014).
[21] J. Paulose, A. S. Meeussen, and V. Vitelli, Proc. Natl. Acad. Sci. U.S.A. **112**, 7639 (2015).
[22] T. Frenzel, C. Findeisen, M. Kadic, P. Gumbsch, and M. Wegener, Adv. Mater. **28**, 5865 (2016).
[23] K. Bertoldi, V. Vitelli, J. Christensen, and M. Van Hecke, Nat. Rev. Mater. **2**, 17066 (2017).
[24] B. McCoy and T. Wu, *The Two-Dimensional Ising Model: Second Edition* (Dover Publications, New York, 2014), ISBN 9780486783123, https://books.google.com/books?id=YO4xAwAAQBAJ.
[25] R. P. Feynman, *Statistical Mechanics: A Set of Lectures* (CRC Press, Boca Raton, FL, 2018).
[26] S. H. Kang, S. Shan, A. Košmrlj, W. L. Noorduin, S. Shian, J. C. Weaver, D. R. Clarke, and K. Bertoldi, Phys. Rev. Lett. **112**, 098701 (2014).
[27] M. E. H. Bahri, S. Sarkar, and A. Košmrlj, arXiv:2209.09350.
[28] P. Z. Hanakata, A. Plummer, and D. R. Nelson, Phys. Rev. Lett. **128**, 075902 (2022).
[29] D. Nelson, T. Piran, and S. Weinberg, *Statistical Mechanics of Membranes and Surfaces* (World Scientific, Singapore, 2004).
[30] See Supplemental Material at http://link.aps.org/supplemental/10.1103/PhysRevLett.130.148201 for movies of typical experiment and simulation, together with details about the performed numerical simulations.
[31] A. P. Thompson, H. M. Aktulga, R. Berger, D. S. Bolintineanu, W. M. Brown, P. S. Crozier, P. J. in't Veld, A. Kohlmeyer, S. G. Moore, T. D. Nguyen *et al.*, Comput. Phys. Commun. **271**, 108171 (2022).
[32] A. P. Thompson, H. M. Aktulga, R. Berger, D. S. Bolintineanu, W. M. Brown, P. S. Crozier, P. J. in't Veld, A. Kohlmeyer, S. G. Moore, T. D. Nguyen *et al.*, Comput. Phys. Commun. **271**, 108171 (2022).
[33] A. Stukowski, Model. Simul. Mater. Sci. Eng. **18**, 015012 (2009).
[34] A. Guerra and D. P. Holmes, Soft Matter **17**, 7662 (2021).
[35] J.-F. Sadoc and R. Mosseri, *Geometrical Frustration* (Cambridge University Press, Cambridge, 1999).
[36] N. Weiner, Y. Bhosale, M. Gazzola, and H. King, J. Appl. Phys. **127**, 050902 (2020).
[37] W. van Adrichem and K. Newman, J. Pet. Technol. **45**, 155 (1993).
[38] G. Gao and S. Z. Miska, SPE J. **14**, 782 (2009).
[39] J. T. Miller, C. G. Mulcahy, J. Pabon, N. Wicks, and P. M. Reis, J. Appl. Mech. **82**, 021003 (2015).
[40] S. Poincloux, T. Chen, B. Audoly, and P. M. Reis, Phys. Rev. Lett. **126**, 218004 (2021).
[41] T. Elder, T. Twohig, H. Singh, and A. B. Croll, Soft Matter **16**, 10611 (2020).
[42] A. B. Croll, Y. Liao, Z. Li, W. M. Jayawardana, T. Elder, and W. Xia, Soft Matter **19**, 1081 (2023).
[43] D. J. Needleman, M. A. Ojeda-Lopez, U. Raviv, K. Ewert, J. B. Jones, H. P. Miller, L. Wilson, and C. R. Safinya, Phys. Rev. Lett. **93**, 198104 (2004).

[44] E. Joselevich, H. Dai, J. Liu, K. Hata, and A. H Windle, *Carbon Nanotubes* (Springer-Verlag Berlin Heidelberg, 2007), pp. 101–165.
[45] E. G. Rakov, Russ. Chem. Rev. **82**, 538 (2013).
[46] L. Wu, Y. Wang, Z. Zhai, Y. Yang, D. Krishnaraju, J. Lu, F. Wu, Q. Wang, and H. Jiang, Appl. Mater. Today **20**, 100671 (2020).
[47] P. Packo, A. N. Norris, and D. Torrent, Phys. Rev. Appl. **15**, 014051 (2021).